Zoology of fractional Chern insulators

Yang-Le Wu, B. Andrei Bernevig, and N. Regnault

Phys. Rev. B **85**, 075116 — Published 14 February 2012

DOI: 10.1103/PhysRevB.85.075116

Zoology of Fractional Chern Insulators

Yang-Le Wu,[1] B. Andrei Bernevig,[1] and N. Regnault[2]

[1]*Department of Physics, Princeton University, Princeton, NJ 08544*
[2]*Laboratoire Pierre Aigrain, ENS and CNRS, 24 rue Lhomond, 75005 Paris, France*

We study four different models of Chern insulators in the presence of strong electronic repulsion at partial fillings. We observe that all cases exhibit a Laughlin-like phase at filling fraction 1/3. We provide evidence of such a strongly correlated topological phase by studying both the energy and the entanglement spectra. In order to identify the key ingredients of the emergence of Laughlin physics in these systems, we show how they are affected when tuning the band structure. We also address the question of the relevance of the Berry curvature flatness in this problem. Using three-body interactions, we show that some models can also host a topological phase reminiscent of the $\nu = 1/2$ Pfaffian Moore-Read state. Additionally, we identify the structures indicating cluster correlations in the entanglement spectra.

PACS numbers: 73.43.-f, 71.10.Fd, 03.65.Vf, 03.65.Ud

I. INTRODUCTION

First introduced by Haldane in his 1988 paper[1], the Chern insulator is the simplest example of a topological insulator. The topological insulating phase is characterized by the (non-zero) Chern number of the occupied band, and it exhibits a non-zero integer Hall conductance σ_{xy} at zero magnetic field. The Hall conductance can be attributed to the metallic edge states protected by the non-trivial topology of the bulk. Interest in such states was boosted by the theoretical prediction[2–5] and subsequent experimental realization[6,7] of time-reversal topological insulators. In its simplest form in two dimensions, this type of insulator consists of two copies (spin up and down) of a Chern insulator. Comprehensive studies have been carried out[8,9], and a complete classification of topological band theories with time-reversal and charge-conjugation symmetries in all dimensions has been established[10–12]. More than two decades after its first introduction, however, the theoretical study of topological insulators is still mostly limited to the single-particle regime, with interaction effects playing a subleading role.

Recent developments have shown that strong electronic interactions open up interesting new possibilities. Novel phases resembling the fractional quantum Hall (FQH) effect have been identified in lattice models at zero magnetic field. Several authors have reported the discovery of the 'fractional Chern insulator' (FCI)[13–15]. They found a FQH phase of interacting electrons on a checkerboard lattice at filling 1/3 and *zero* magnetic field. The feature of this phase is an almost 3-fold degenerate incompressible ground state with Hall conductance $\sigma_{xy} = 1/3$, reminiscent of the FQH Laughlin state on a torus. A similar state has been found on a triangular lattice as well[16]. In parallel, FCI phases of interacting bosons have been realized[17,18], a time-reversal-symmetric fractional topological liquid state has been constructed from two copies of FCI[19,20], and an integer quantum Hall effect has been found in a half-filled Hubbard model in coexistence with an Ising ferromagnetic order[21].

The resemblance of the FCI phase to the conventional FQH effect has been justified from several perspectives. First, the FCI phase has quasiparticle excitations with fractional statistics[15,22], and the quasiparticles are governed by the admissible counting rules first found in the study of the FQH effect[23,24]. Second, in the limit of long wavelength and uniform Berry curvature, the projected single-particle density operators form a closed Lie algebra[25,26]. This algebra has the same structure as the Girvin-MacDonald-Platzman algebra of magnetic translations and projected density operators in the FQH effect[27]. Third, Wannier functions maximally localized in one dimension have been explicitly constructed from the single-particle states of a Chern band[28]. Finally, various constructions of FQH-analogue wave-functions for the ground state of FCI have been proposed, using either Wannier functions[28] or a parton approach[29–31].

In this paper we show that the FCI phase is present in the Haldane model on the honeycomb lattice[1], in a two-orbital model that resembles half (spin-up) of the Mercury-Telluride two-dimensional topological insulator[5], in the Kagome lattice model with spin-orbit coupling[32], and in the spin-polarized ruby lattice model[33]. These models allow us to study FCI in different physical situations such as different lattices or different number of Bloch bands. Working in a single flattened band, we find in each model a more or less robust Laughlin FQH phase at 1/3 filling in the presence of repulsive two-body nearest-neighbor interactions. The 3-fold degenerate ground states are separated from the excited states by a finite gap and flow into each other upon flux insertion with a period of 3 fluxes. This signals a Hall conductance $\sigma_{xy} = 1/3$. We identify hallmarks of fractional excitations of the Laughlin 1/3 universality class in the energy spectrum as well as the entanglement spectrum. We then discuss the stability of the topological ground state under parameter variation, and test its correlation with the anisotropy of the Berry curvature. We also show that another FCI phase reminiscent of the Pfaffian Moore-Read FQH state[34] is present in the Kagome and ruby lattice models at half filling of the valence band. Finally,

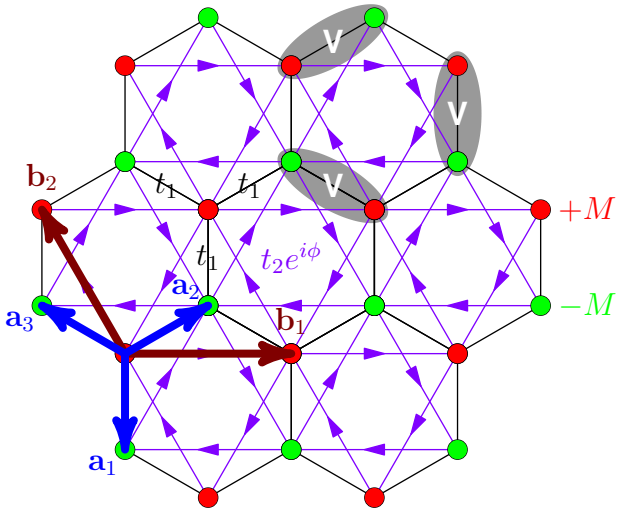

FIG. 1: The Haldane model on the honeycomb lattice. A and B sublattices are colored in red and green, respectively. The lattice translation vectors are $\mathbf{b}_1 = \mathbf{a}_2 - \mathbf{a}_3$ and $\mathbf{b}_2 = \mathbf{a}_3 - \mathbf{a}_1$. The hopping between NN is t_1, and the hopping between NNN is $t_2 e^{i\phi}$ in the direction of arrows. The density-density repulsion between nearest neighbors is depicted in gray ellipses.

we highlight several structures in the higher levels of the particle entanglement spectrum[35,36] of the ground state at filling 1/3 that may serve as a hint for the stable existence of other FQH states at other fillings, such as the Read-Rezayi series[37].

II. HALDANE MODEL

The Haldane model[1] is the first studied example of a topological insulator. We would like to see if this model can host fermionic FCI phases (the bosonic version has recently been reported in Refs. 17,18). We adopt the honeycomb lattice layout from Ref. 13. As shown in Fig. 1, the two sublattices A and B are connected by the vectors $\mathbf{a}_1 = (0, -1)$, $\mathbf{a}_2 = (\sqrt{3}/2, 1/2)$, $\mathbf{a}_3 = (-\sqrt{3}/2, 1/2)$. We define the lattice translation vectors $\mathbf{b}_1 = \mathbf{a}_2 - \mathbf{a}_3$, $\mathbf{b}_2 = \mathbf{a}_3 - \mathbf{a}_1$. The Haldane model[1] has real hopping amplitude t_1 between nearest neighbors (NN), complex hopping amplitude $t_2 e^{\pm i\phi}$ between next-nearest neighbors (NNN), and an inversion-breaking sublattice potential M.

After a Fourier transform to the first Brillouin zone and a gauge transform on the B sublattice $\psi_{\mathbf{k},B} \to e^{i\mathbf{k}\cdot(\mathbf{b}_1+2\mathbf{b}_2)/3}\psi_{\mathbf{k},B}$, the single-particle Hamiltonian can be put in Bloch form as $H = \sum_{\mathbf{k}} (\psi^\dagger_{\mathbf{k},A}, \psi^\dagger_{\mathbf{k},B}) h(\mathbf{k}) (\psi_{\mathbf{k},A}, \psi_{\mathbf{k},B})^{\mathrm{T}}$. Here the lattice momentum $\mathbf{k} = (\mathbf{k}\cdot\mathbf{b}_1, \mathbf{k}\cdot\mathbf{b}_2) \equiv (k_x, k_y)$ is summed over the first Brillouin zone, and the $h(\mathbf{k})$ matrix can be expressed in terms of the identity and 3 Pauli matrices, $h(\mathbf{k}) = d_0 \mathbb{I} + \sum_i d_i \sigma_i$, where

$$\begin{aligned} d_0 &= 2t_2 \cos\phi[\cos k_x + \cos k_y + \cos(k_x + k_y)], \\ d_x &= t_1[1 + \cos(k_x + k_y) + \cos k_y], \\ d_y &= t_1[-\sin(k_x + k_y) - \sin k_y], \\ d_z &= M + 2t_2 \sin\phi[\sin k_x + \sin k_y - \sin(k_x + k_y)]. \end{aligned} \tag{1}$$

The single-particle Hamiltonian has inversion symmetry at $M = 0$ and the 3-fold point group symmetry of the honeycomb lattice. At $M = 0$, inversion exchanges the two sublattices and transforms the annihilation operators by $(\psi_{\mathbf{k},A}, \psi_{\mathbf{k},B})^{\mathrm{T}} \to \sigma_x(\psi_{-\mathbf{k},A}, \psi_{-\mathbf{k},B})^{\mathrm{T}}$. The 3-fold rotation generates the cyclic permutation of the lattice translation vectors $\mathbf{b}_1 \to \mathbf{b}_2 \to -\mathbf{b}_1 - \mathbf{b}_2 \to \mathbf{b}_1$ on each sublattice and thus transforms the wave vectors by $(k_x, k_y) \to (k_y, -k_x - k_y)$. Therefore, the Bloch Hamiltonian has the following two symmetries:

$$\begin{aligned} h(k_x, k_y) &= \sigma_x h(-k_x, -k_y)\sigma_x, \\ h(k_x, k_y) &= U^\dagger(k_x, k_y) h(k_y, -k_x - k_y) U(k_x, k_y), \end{aligned} \tag{2}$$

where $U(k_x, k_y)$ is a diagonal 2×2 unitary matrix, with $[1, e^{i(k_x+k_y)}]$ on the diagonal. When the system is put on the lattice of finite size $N_x \times N_y$ with periodic boundary, the 3-fold rotation symmetry is lifted, unless $N_x = N_y$.

To focus on the effect of interactions without being distracted by single-particle dispersion, we always take the flat-band limit of the insulator, i.e. replace the original Bloch Hamiltonian $h(\mathbf{k}) = \sum_n E_n(\mathbf{k}) P_n(\mathbf{k})$ by $\sum_n E_n(0) P_n(\mathbf{k})$, where $P_n(\mathbf{k})$ is the projector onto the n-th band. We then send the band gap to infinity and work directly in the lowest band, in the same spirit of the lowest Landau level projection routinely adopted in the FQH literature. We then add a density-density repulsion between nearest neighbors. Since a flattened band does not provide an energy scale, we are free to set the interaction strength to unity. After the aforementioned gauge transform on $\psi_{\mathbf{k},B}$, the interaction term can be written in the sublattice basis as

$$\frac{1}{N} \sum_{\{\mathbf{k}_i\}} \psi^\dagger_{\mathbf{k}_3 A} \psi^\dagger_{\mathbf{k}_4 B} \psi_{\mathbf{k}_2 B} \psi_{\mathbf{k}_1 A} \delta^{\mathrm{mod}2\pi}_{\mathbf{k}_1+\mathbf{k}_2-\mathbf{k}_3-\mathbf{k}_4} V_{\mathbf{k}_1\mathbf{k}_2\mathbf{k}_3\mathbf{k}_4}, \tag{3}$$

where

$$V_{\mathbf{k}_1\mathbf{k}_2\mathbf{k}_3\mathbf{k}_4} = 1 + e^{i(\mathbf{k}_2-\mathbf{k}_4)\mathbf{b}_2} + e^{i(\mathbf{k}_2-\mathbf{k}_4)(\mathbf{b}_1+\mathbf{b}_2)}, \tag{4}$$

as illustrated in Fig. 1.

A. Ground state at 1/3 filling

We diagonalize the interacting Hamiltonian in the flattened lowest band at filling 1/3. We show the energy spectrum of $N = 8, 10, 12$ particles on the $N_x \times N_y = 6 \times \frac{N}{2}$ lattice in Fig. 2. The calculations are performed with $(t_1, t_2, M, \phi) = (1, 1, 0, 0.13)$. The particular choice of parameters will be discussed later. In the three cases ($N =$

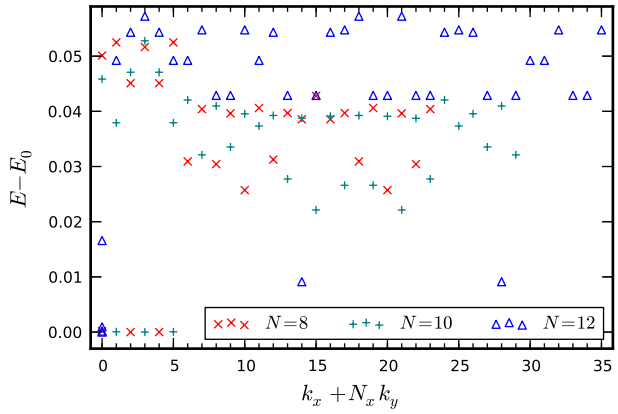

FIG. 2: Low energy spectrum of the Haldane model with $N = 8$ (marked by red crosses), $N = 10$ (green plus signs), and $N = 12$ (blue triangles) particles on the $N_x \times N_y = 6 \times \frac{N}{2}$ lattice, with energies shifted by E_0, the lowest energy for each system size. We only show the lowest excited level in each momentum sector in addition to the 3-fold ground state.

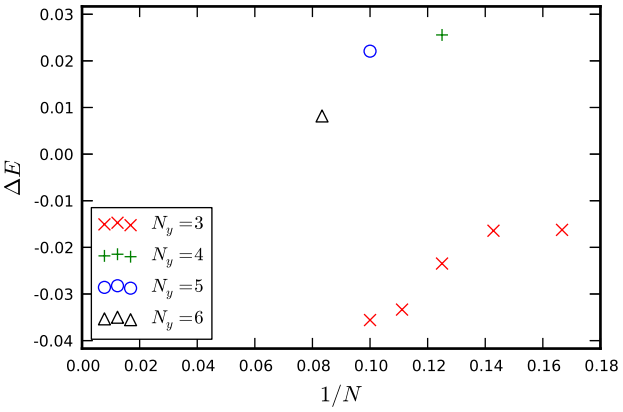

FIG. 3: Energy gap ΔE for different system sizes and aspect ratios of the Haldane model. The gap is defined as the energy difference between the first excited state and the highest of the 3-fold ground states. A more precise definition of ΔE is given in Section II D. In each case, $N_x = 3N/N_y$. The negative values of ΔE in the $N_y = 3$ group mean that the actual ground state is not in the momentum sectors predicted by the theoretical counting rule, i.e. the gap above the supposed topological ground state closes.

8, 10, 12), a 3-fold degenerate ground state is seen at total momenta $\{(0,0),(2,0),(4,0)\}$, $\{(1,0),(3,0),(5,0)\}$, and $\{(0,0),(0,0),(0,0)\}$, respectively. This agrees perfectly with the $(1,3)$-admissible counting proposed in Ref. 15 and recently developed in Ref. 22. The finite-size scaling of the energy gap ΔE is shown in Fig. 3. The energy gap does not seem to remain open in the thermodynamic limit even if the aspect ratio N_x/N_y remains finite. Nonetheless, as discussed in the following sections, we find solid evidence for the topological nature of the ground state; the detailed investigation into the energetics will be presented in future work.

The three degenerate ground states exhibit spectral

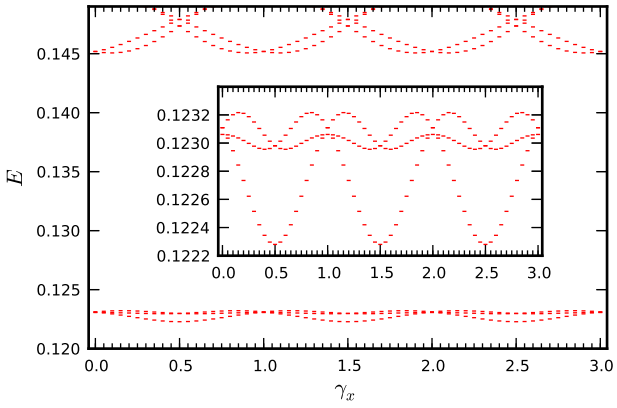

FIG. 4: Spectral flow of the low-lying states of the Haldane model with $N = 10$ particles on the $N_x \times N_y = 6 \times 5$ lattice upon flux insertion along the x direction. γ_x counts the number of fluxes inserted. The 3-fold ground states flow into each other, and do not mix with higher states during flux insertion. It takes 3 full fluxes for the 3-fold states to return to the original configuration (inset).

flow upon flux insertion. For example, inserting a unit flux in the x direction shifts the single particle momentum $k_x \to k_x + 2\pi\gamma_x$, with γ_x going from 0 to 1; this induces the spectral flow within the 3-fold ground state (Fig. 4). Upon insertion of 3 full fluxes, the 3 degenerate states restore their original configuration. Given the unit Chern number of the valence band, we conclude the system has Hall conductance $\sigma_{xy} = 1/3$.

We have also checked the effect of density-density repulsion between NNN on the 1/3 phase. Overall, this additional interaction term weakens the Laughlin-like phase. These results are in agreement with those of Sheng et al.[14] for the checkerboard model.

B. Quasihole excitations

Three-fold degeneracy alone is insufficient to fully establish the observed ground state as a FQH state; it could very well be an imprint of a lattice charge density wave. To rule out this alternative we need to study the excitations of the system. We decrease the filling ν from 1/3 and check for quasiholes in the energy spectrum. In Fig. 5 we show the energy spectrum of $N = 7$ particles on the $N_x \times N_y = 6 \times 4$ lattice, and in Fig. 6 the energy spectrum of $N = 9$ particles on the $N_x \times N_y = 6 \times 5$ lattice. (We run into convergence problems at $N = 11$.) These configurations have the same lattice geometry as the corresponding ground states shown earlier, but with one electron removed. An energy gap is clearly visible in the spectrum, and the low-energy part has the same counting in each momentum sector as predicted by the $(1,3)$-admissible rule. This further substantiates that the ground state observed at filling 1/3 indeed has the basic features of the Laughlin FQH state[38].

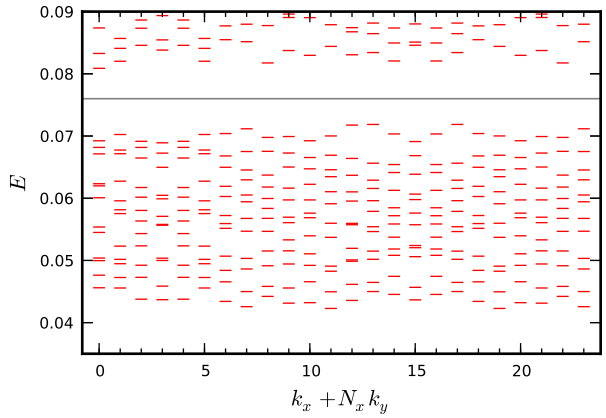

FIG. 5: Low energy spectrum of the Haldane model with $N = 7$ particles on the $N_x \times N_y = 6 \times 4$ lattice. The number of states below the gray line is 12 in each momentum sector, in agreement with the $(1, 3)$-admissible counting rule.

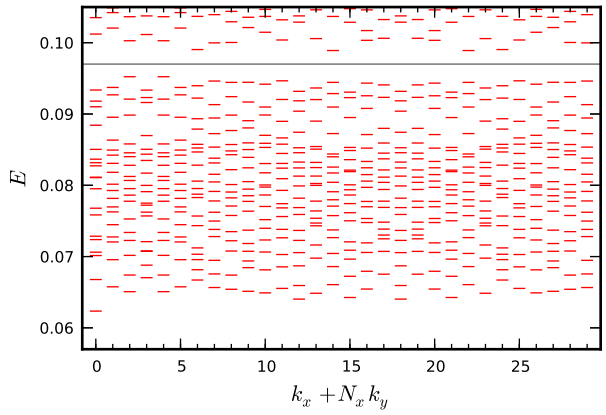

FIG. 6: Low energy spectrum of the Haldane model with $N = 9$ particles on the $N_x \times N_y = 6 \times 5$ lattice. The number of states below the gray line is 19 in momentum sectors with $k_x = 0, 3$ and 18 elsewhere, in agreement with the $(1, 3)$-admissible counting rule.

C. Entanglement spectrum

Recent developments[35,36,39] showed that the excitations in FQH systems are manifested in the entanglement between particles[35,40–42] in the many-body ground state. Using this alternative probe, we provide further evidence that the ground state at filling 1/3 is a FQH Laughlin state. This tool is highly valuable in the present case since no overlap with model wave functions can be computed: despite several proposals[28–31], concrete expressions for the model wave functions have not been established for FCI.

Specifically, we cut the system in the way described in Ref. 36 and further used to look at the FCIs in Ref. 15. We divide N particles into two subsystem of N_A and N_B particles, and trace out the degrees of freedom carried by the N_B particles. The eigenvalues $e^{-\xi}$ of the resulting reduced density matrix $\rho_A = \mathrm{Tr}_B \rho = \mathrm{Tr}_B |\psi\rangle\langle\psi|$ define the

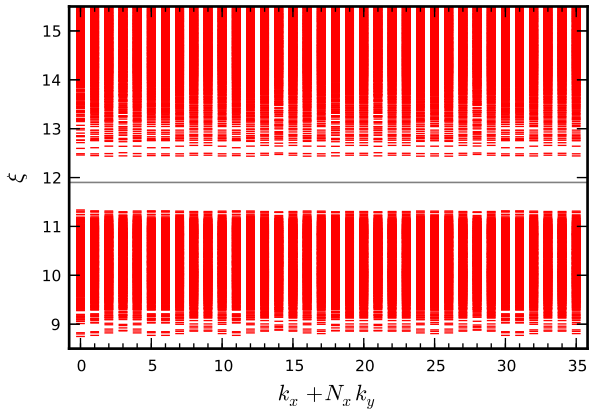

FIG. 7: Particle entanglement spectrum of the ground state of the Haldane model of $N = 12$ particles on the $N_x \times N_y = 6 \times 6$ lattice, with $N_B = 8$ particles traced out. The number of states below the gray line is 741 in momentum sectors where both k_x and k_y are even and 728 elsewhere, in agreement with the $(1, 3)$-admissible counting rule. The system size is exactly the same as Fig. 13 of Ref. 15.

particle entanglement energies ξ. For degenerate ground states, we form the density matrix as an incoherent sum with equal weights[15] $\rho = \frac{1}{3}\sum_i |\psi_i\rangle\langle\psi_i|$. Then, the entanglement energy levels ξ can be displayed in groups marked by the total momentum (k_x, k_y) of the N_A particles. A typical case is shown in Fig. 7. The spectrum is very similar to what was found in the checkerboard lattice model[15]. We observe a clear, although narrower, entanglement gap in the spectrum; the counting of the entanglement energy levels below the gap matches (in each momentum sector) the $(1, 3)$-admissible quasihole counting[22] of N_A particles on the $N_x \times N_y$ reciprocal lattice. We have checked all values of N_A manageable by current computers and have found perfect agreement with the counting principle in all cases. Given the vast difference between the checkerboard lattice model and the Haldane model (lattice symmetry, coordination number, flux distribution, etc.), the similarity in the entanglement spectrum is surprising. Compared with the relatively fuzzy quasihole energy spectrum, the ground state entanglement spectrum turns out to be a more reliable alternative route to probe the physics of fractional excitations.

D. Parameter dependence

As analyzed by Haldane[1], strong inversion breaking eventually overcomes the non-trivial topology; the Chern number vanishes when $|M| > 3\sqrt{3}|t_2 \sin\phi|$. We now study whether strong interactions would further shrink the volume of the topologically non-trivial phase in parameter space. The density-density interaction projected to the flattened valence band has two parametric degrees of freedom $(M/t_1, t_2 \sin\phi/t_1)$, which effectively change the Berry curvature in the model. Without loss of gener-

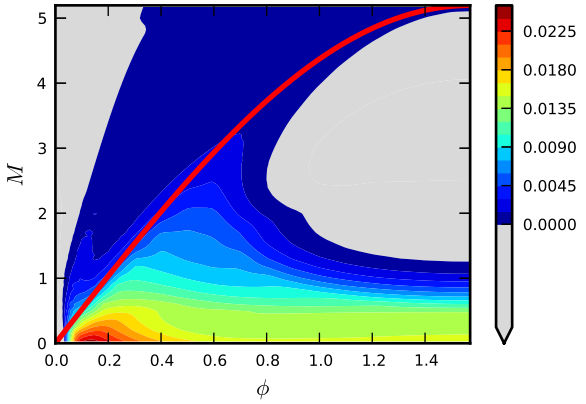

FIG. 8: The distribution of the energy gap ΔE in the (ϕ, M) plane for the Haldane model of $N = 8$ particles on the $N_x \times N_y = 6 \times 4$ lattice. The color code for ΔE is shown by the bar on the right, and the region with the gap closed is marked in gray. The bold red line $M = 3\sqrt{3}\sin\phi$ separates the topologically non-trivial sector of the single-particle problem from the trivial one.

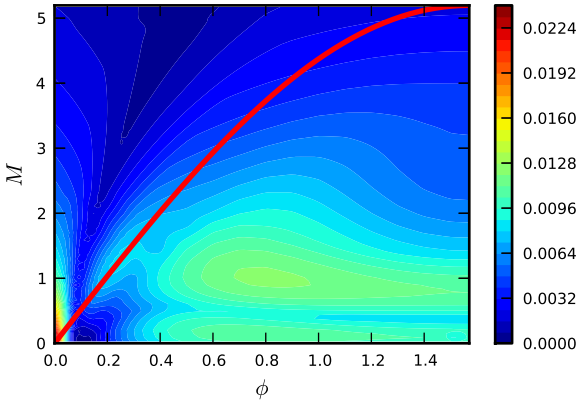

FIG. 9: The distribution of the energy spread δE in the (ϕ, M) plane for the Haldane model of $N = 8$ particles on the $N_x \times N_y = 6 \times 4$ lattice. The color code for δE is shown by the bar on the right. The bold red line $M = 3\sqrt{3}\sin\phi$ separates the topologically non-trivial sector of the single-particle problem from the trivial one.

ality, we fix $t_1 = t_2 = 1$ and study the region with $M > 0$ and $\phi \in [0, \pi/2]$. There is no clear boundary between different interacting phases in finite-size numerics. We thus need a quantitative characterization of the similarity to the ideal FCI state.

We denote the $(1, 3)$-admissible counting of N particles on the $N_x \times N_y$ lattice in momentum sector (k_x, k_y) by n_{k_x,k_y}^{N,N_x,N_y}. We denote by $\mathcal{A}$ the collection of the lowest n_{k_x,k_y}^{N,N_x,N_y} states in each momentum sector, and by $\bar{\mathcal{A}}$ the collection of all the other states. If the system is in a well-developed FCI state, the collection $\mathcal{A}$ is the 3-fold degenerate ground state, while the collection $\bar{\mathcal{A}}$ contains the excited states. The energy gap is thus $\Delta E = \min E_{\bar{\mathcal{A}}} - \max E_{\mathcal{A}}$, and the energy spread of the ground-state manifold can be defined as $\delta E = \max E_{\mathcal{A}} - \min E_{\mathcal{A}}$. Further, we calculate the entanglement spectra of the degenerate ground state for various partitions (N_A, N_B) of N particles. For each N_A, we denote by $\mathbb{A}$ the collection of the lowest $n_{k_x,k_y}^{N_A,N_x,N_y}$ entanglement energy levels in each momentum sector, and by $\bar{\mathbb{A}}$ all the other entanglement energy levels. We define the entanglement gap $\Delta\xi = \min \xi_{\bar{\mathbb{A}}} - \max \xi_{\mathbb{A}}$. The parameter sets with large ΔE, small δE and large $\Delta\xi$ are likely to host a FCI state.

In Figs. 8, 9, 10, we show the distribution of ΔE, δE, $\Delta\xi$ over the (ϕ, M) plane. Combining the three plots, we find that the region enclosed by $|M| < 3\sqrt{3}|t_2 \sin\phi|$ and $|M| \lesssim 3\sqrt{3}|t_2|(0.4 - |\sin\phi|)$ has large ΔE and $\Delta\xi$, and small δE, and hence is likely to support a FCI phase.

E. Berry curvature variation

A few authors pointed out that a Chern band shares an important feature with the Landau level[22,25,26]. In

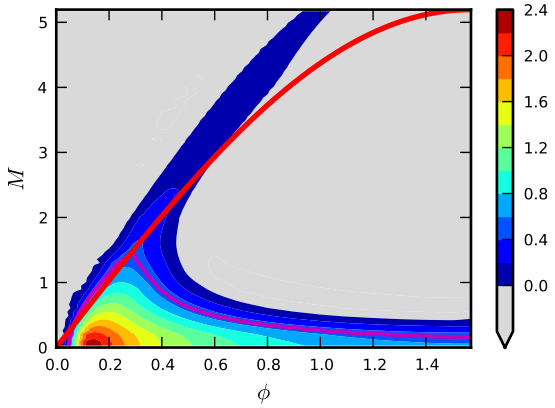

FIG. 10: The distribution of the entanglement gap $\Delta\xi$ in the (ϕ, M) plane for the ground state of the Haldane model of $N = 8$ particles on the $N_x \times N_y = 6 \times 4$ lattice, with $N_B = 5$ particles traced out. The color code for $\Delta\xi$ is shown by the bar on the right, and the region with the gap closed is marked in gray. The average spacing of the entanglement levels below the gap is at most 0.05 (not shown in the figure); hence the entanglement gap should be considered widely open as long as $\Delta\xi \gg 0.05$. The line with $\Delta\xi = 0.5$ is shown in magenta. The bold red line $M = 3\sqrt{3}\sin\phi$ separates the topologically non-trivial sector of the single-particle problem from the trivial one.

the limit of long wave-length and uniform Berry curvature, the projected density operators form a closed Lie algebra. This algebra has the same structure as the Girvin-MacDonald-Platzman algebra of magnetic translations[27], with the Berry curvature taking the role of the uniform magnetic field. They thus argued that the development of the FCI phase is driven by this algebraic structure. This picture suggests a negative correlation between Berry curvature fluctuations and the propensity towards a FCI phase. This is indeed observed in finite-

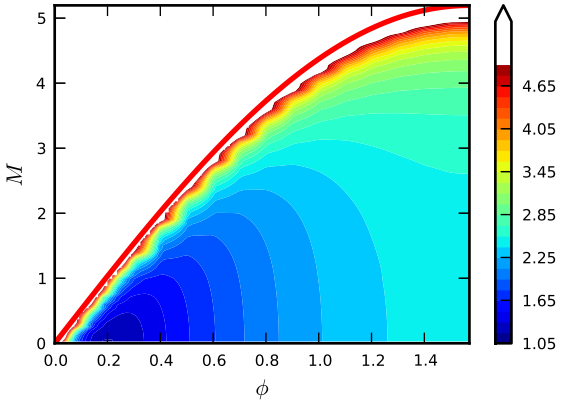

FIG. 11: The distribution of the standard deviation of the Berry curvature $\sigma_{\mathcal{B}}$ in the (ϕ, M) plane for the Haldane model of $N = 8$ particles on the $N_x \times N_y = 6 \times 4$ lattice. The bar on the right shows the color code for the value of $2\pi\sigma_{\mathcal{B}}$. The bold red line $M = 3\sqrt{3}\sin\phi$ separates the topologically non-trivial sector of the single-particle problem from the trivial one. We focus on the non-trivial sector. The strong fluctuation of the Berry curvature very close to the boundary of the non-trivial sector is not shown.

size numerics, as we describe below.

We measure Berry curvature fluctuations by the simplest possible option, its standard deviation $\sigma_{\mathcal{B}}$ in units of the average Berry curvature $|\bar{\mathcal{B}}| = 1/2\pi$. The distribution of $2\pi\sigma_{\mathcal{B}}$ is shown in Fig. 11. Comparing this with the patterns in Figs. 8, 9, 10, we find a clear correlation between $\sigma_{\mathcal{B}}$ and the three measures of the propensity towards the FCI phase over the full range of the parameter scan. In particular, the optimal parameter region supporting a robust FCI phase coincides with the part of the parameter space with least fluctuating Berry curvature. While this agrees with the picture we expect from the algebraic structure[22,25,26,43], we stress that the fluctuation at the optimal parameters is still quite significant, with its standard deviation comparable to the mean value. The FCI is apparently more robust to Berry curvature fluctuations than expected. This is crucial for two-band Chern insulators since their Berry curvature cannot be completely flat due to the no-hair theorem[44].

III. TWO-ORBITAL MODEL

We now turn to a simpler model with two orbitals on each site of a square lattice. This model represents the spin-up half of the Mercury-Telluride two-dimensional topological insulator[5]. As shown in Fig. 12, there are two orbitals A, B on each site, with energy difference $2M$. The intra-orbital NN hopping has amplitude $\pm t_2$, while the inter-orbital NN hopping has amplitude $\pm it_1$ and $\pm t_1$ in the x and y directions, respectively. These amplitudes have been specifically designed such that the single-particle Bloch Hamiltonian takes the form $H = \sum_{\mathbf{k}}(\psi^\dagger_{\mathbf{k},A}, \psi^\dagger_{\mathbf{k},B})h(\mathbf{k})(\psi_{\mathbf{k},A}, \psi_{\mathbf{k},B})^{\mathrm{T}}$, where

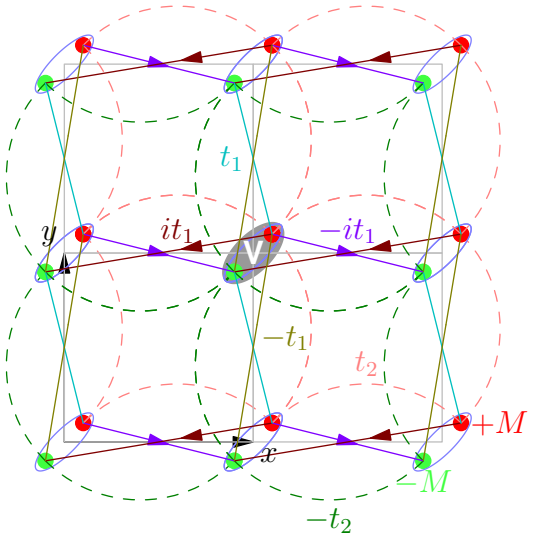

FIG. 12: The two-orbital model on square lattice. The two orbitals A,B are colored in red and green, respectively. The intra-orbital NN hopping amplitude is t_2 between the A orbitals, and $-t_2$ between the B orbitals. The inter-orbital NN hopping amplitude is $\pm it_1$ in the x direction along the arrows, and $\pm t_1$ in the y direction. The on-site Hubbard repulsion is depicted by the ellipse in gray.

$$h(\mathbf{k}) = 2t_1 \sin k_x \sigma_x + 2t_1 \sin k_y \sigma_y + [M - 2t_2(\cos k_x + \cos k_y)]\sigma_z. \quad (5)$$

Similar to the case of the Haldane model, we can flatten the Bloch bands using projectors. We then add Hubbard inter-orbital repulsion to each site, as shown in Fig. 12. In momentum space, the interaction term reads

$$\frac{1}{N}\sum_{\{\mathbf{k}_i\}} \delta^{\mathrm{mod}2\pi}_{\mathbf{k}_1+\mathbf{k}_2-\mathbf{k}_3-\mathbf{k}_4} \psi^\dagger_{\mathbf{k}_3 A}\psi^\dagger_{\mathbf{k}_4 B}\psi_{\mathbf{k}_2 B}\psi_{\mathbf{k}_1 A}. \quad (6)$$

Even though at single-particle level a two-orbital-per-site model is equivalent to a model with two sites in each unit cell, this situation changes when interactions are included. Notice that the interaction here (Eq. 6) has a different form factor than the one in Eq. 4.

We diagonalize the interacting Hamiltonian in the flattened lowest band at filling 1/3 and $(t_2/t_1, M/t_1) = (1, 2)$. We show the energy spectrum of $N = 8, 10$ particles on the $N_x \times N_y = 6 \times \frac{N}{2}$ lattice in Fig. 13. (We run into serious convergence problems at $N = 12$.) In the two cases ($N = 8, 10$), a 3-fold degenerate ground state is seen at total momenta $\{(0,0),(2,0),(4,0)\}$ and $\{(1,0),(3,0),(5,0)\}$, respectively. This agrees perfectly with the $(1,3)$-admissible counting proposed in Ref. 15, 22. As shown in Fig. 14, the energy gap ΔE remains open and scales to a finite value in the limit of $N \to \infty$ with N_x/N_y finite. The three degenerate ground states exhibit spectral flow upon flux insertion with a period of 3 fluxes (see Fig. 15). This shows that the system

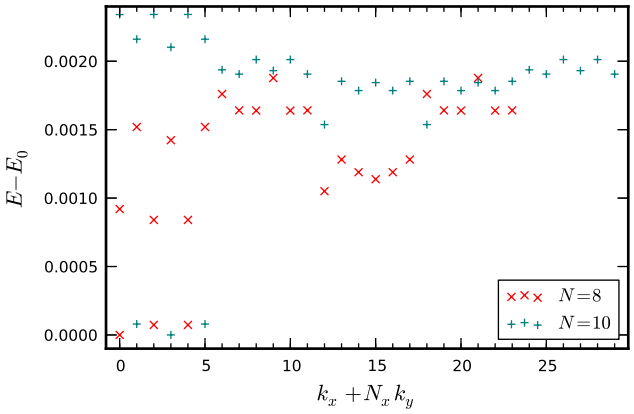

FIG. 13: Low energy spectrum of two-orbital model for $N = 8$ (marked by red crosses) and $N = 10$ (green plus signs) particles on $(N_x, N_y) = (6, N/2)$ lattice, with energies shifted by E_0, the lowest energy for each system size. We only show the lowest excited level in each momentum sector in addition to the 3-fold ground state.

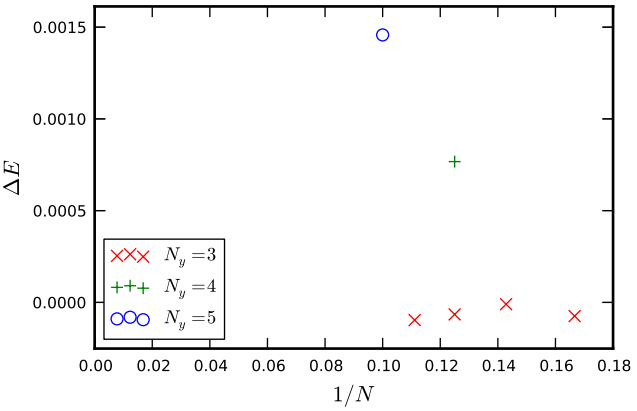

FIG. 14: Energy gap ΔE of the two-orbital model for different system sizes and aspect ratios. In each case, $N_x = 3N/N_y$. The negative values of ΔE in the $N_y = 3$ group mean that the actual ground state is not in the momentum sectors predicted by the theoretical counting rule.

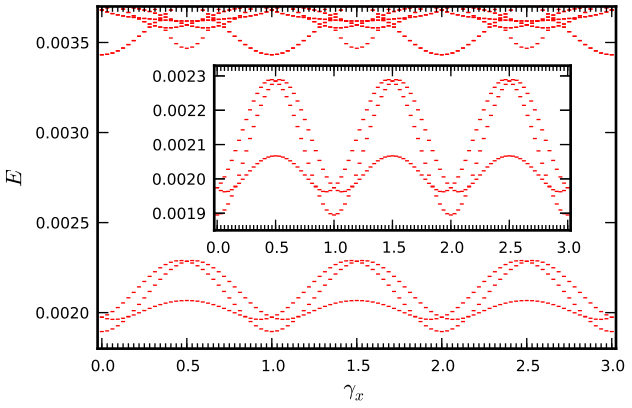

FIG. 15: Spectral flow of the low-lying states of the two-orbital model with $N = 10$ particles on the $N_x \times N_y = 6 \times 5$ lattice upon flux insertion along the x direction. γ_x counts the number of fluxes inserted. The 3-fold ground states flow into each other, and do not mix with higher states during flux insertion. It takes 3 full fluxes for the 3-fold states to return to the original configuration (inset).

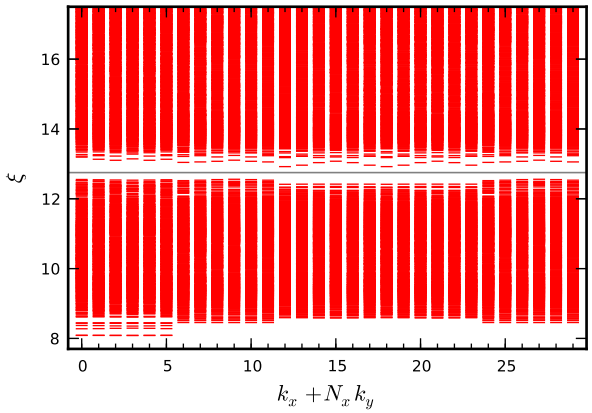

FIG. 16: Particle entanglement spectrum of the ground state of the two-orbital model of $N = 10$ particles on the $N_x \times N_y = 6 \times 5$ lattice, with $N_B = 5$ particles traced out. The number of states below the gray line is 776 in momentum sectors with $k_y = 0$ and 775 in all the other sectors, in agreement with the analytical counting rule.

has Hall conductance $\sigma_{xy} = 1/3$. We study the quasihole excitations through ground state entanglement. In Fig. 16, we observe an entanglement gap in the spectrum. The counting of the entanglement energy levels below the gap again matches in each momentum sector the $(1, 3)$-admissible counting. This shows that the excitations in the ground state of the two-orbital model have the same counting as that of Abelian fractional statistics $1/3$ quasiholes. We thus conclude that the ground state is a FQH Laughlin state.

The two-orbital model has topologically non-trivial bands when $|M| < 4|t_2|$. We now move the system away from the point $(t_2, M) = (1, 2)$ and probe this parameter region. In Figs. 17, 18, 19, we display the distribution of the energy gap ΔE, the energy spread δE, and the entanglement gap $\Delta\xi$ of the ground state. Compared with the Haldane model, the situation is more complicated. The maximum of the energy gap ΔE does not coincide with the minimum of the energy spread δE. Rather, the region with large gap ΔE tends to have large spread δE as well. The peak of the entanglement gap $\Delta\xi$ is close neither to the maximum of ΔE nor to the minimum of δE. Varying (M, t_2) scans over the manifold of the two-orbital interacting Hamiltonians projected to the lowest band. The lack of correlation between ΔE, δE and $\Delta\xi$ suggests that the distance from this manifold of Hamiltonians to the Laughlin model Hamiltonian is quite large. Further, we check the correlation between Berry curvature fluctuations and the propensity towards the FCI phase. The variation of the curvature fluctuation is shown in Fig. 20. We observe weak correlation between

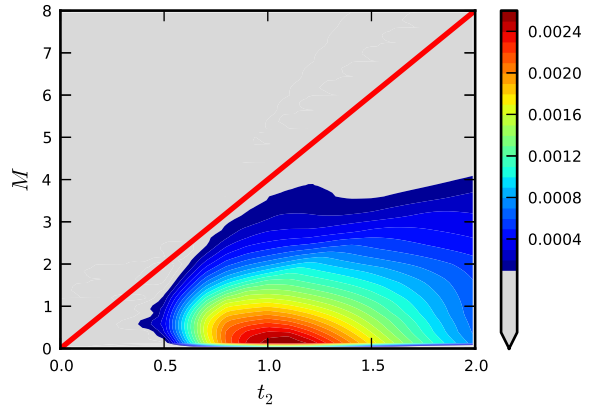

FIG. 17: The distribution of the energy gap ΔE in the (t_2, M) plane for the two-orbital model of $N = 8$ particles on the $N_x \times N_y = 6 \times 4$ lattice. The color code for ΔE is shown by the bar on the right, and the region with the gap closed is marked in gray. The bold red line $M = 4t_2$ separates the topologically non-trivial sector of the single-particle problem from the trivial one.

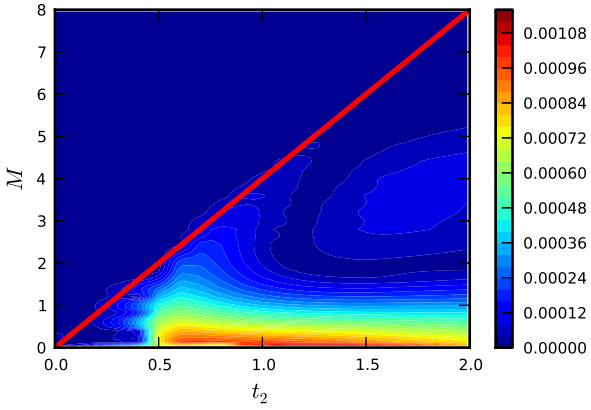

FIG. 18: The distribution of the energy spread δE in the (t_2, M) plane for the two-orbital model of $N = 8$ particles on the $N_x \times N_y = 6 \times 4$ lattice. The color code for δE is shown by the bar on the right. The bold red line $M = 4t_2$ separates the topologically non-trivial sector of the single-particle problem from the trivial one.

$\sigma_{\mathcal{B}}$ and δE and find little association between $\sigma_{\mathcal{B}}$ and ΔE or $\Delta\xi$. It is possible that $\sigma_{\mathcal{B}}$ is not a very good measure of the Berry curvature fluctuation. We note that in this model the interaction before projection is constant. We leave in-depth study of this issue for future work.

IV. KAGOME LATTICE MODEL

We study the Kagome lattice model built by Tang et al.[32]. As shown in Fig. 21, the lattice is spanned by the translation vectors $\mathbf{b}_1$ and $\mathbf{b}_2$, and it consists of three sublattices A,B,C. In Ref. 32, the single-particle model has been studied both without and with NNN hopping terms. We have looked at the effect of interactions in both cases. But for sake of simplicity we focus mostly on the case without NNN hoppings. The hopping amplitude between NN is $t_1 \pm i\lambda_1$. After a Fourier transform and a gauge transform $\psi_{\mathbf{k},B} \to \psi_{\mathbf{k},B} e^{-i\mathbf{k}\cdot\mathbf{b}_1/2}$, $\psi_{\mathbf{k},C} \to \psi_{\mathbf{k},C} e^{-i\mathbf{k}\cdot\mathbf{b}_2/2}$, the single-particle Hamiltonian can be cast in Bloch form as $H = \sum_{\mathbf{k}} (\psi^\dagger_{\mathbf{k},A}, \psi^\dagger_{\mathbf{k},B}, \psi^\dagger_{\mathbf{k},C}) h(\mathbf{k}) (\psi_{\mathbf{k},A}, \psi_{\mathbf{k},B}, \psi_{\mathbf{k},C})^{\mathrm{T}}$. Here the lattice momentum $\mathbf{k} = (\mathbf{k}\cdot\mathbf{b}_1, \mathbf{k}\cdot\mathbf{b}_2) \equiv (k_x, k_y)$ is summed

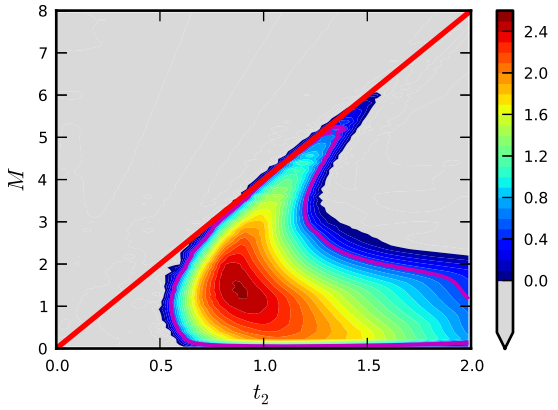

FIG. 19: The distribution of the entanglement gap $\Delta\xi$ in the (t_2, M) plane for the ground state of the two-orbital model of $N = 8$ particles on the $N_x \times N_y = 6 \times 4$ lattice, with $N_B = 5$ particles traced out. The color code for $\Delta\xi$ is shown by the bar on the right, and the region with the gap closed is marked in gray. The average spacing of the entanglement levels below the gap is at most 0.05 (not shown in the figure); hence the entanglement gap should be considered widely open as long as $\Delta\xi \gg 0.05$. The line with $\Delta\xi = 0.5$ is shown in magenta. The bold red line $M = 4t_2$ separates the topologically non-trivial sector of the single-particle problem from the trivial one.

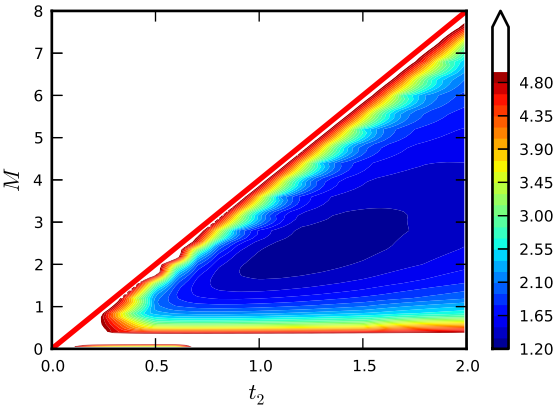

FIG. 20: The distribution of the standard deviation of the Berry curvature $\sigma_{\mathcal{B}}$ in the (t_2, M) plane for the two-orbital model of $N = 8$ particles on the $N_x \times N_y = 6 \times 4$ lattice. The bar on the right shows the color code for the value of $2\pi\sigma_{\mathcal{B}}$. The bold red line $M = 4t_2$ separates the topologically non-trivial sector of the single-particle problem from the trivial one. We focus on the non-trivial sector. The strong fluctuation of the Berry curvature very close to the boundary of the non-trivial sector is not shown.

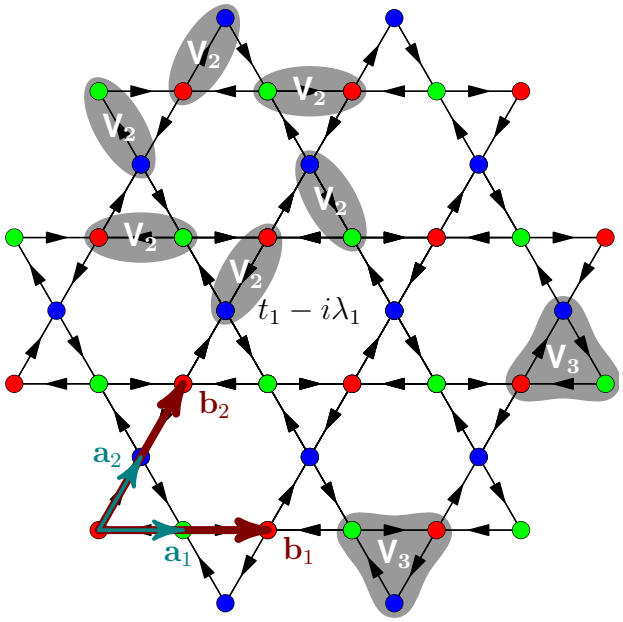

FIG. 21: The Kagome lattice model with NN spin-orbit coupling. The three sublattices A,B,C are colored in red, green, blue, respectively. The lattice translation vectors are $\mathbf{b}_1 = 2\mathbf{a}_1$, $\mathbf{b}_2 = 2\mathbf{a}_2$. The hopping amplitude between NN is $t_1 - i\lambda_1$ in the direction of arrows. The two-body and the three-body interactions between NN are illustrated by the gray ellipses and triangles, respectively.

over the first Brillouin zone, and the $h(\mathbf{k})$ matrix reads

$$h(\mathbf{k}) = -t_1 \begin{bmatrix} 0 & 1+e^{-ik_x} & 1+e^{-ik_y} \\ 1+e^{ik_x} & 0 & 1+e^{i(k_x-k_y)} \\ 1+e^{ik_y} & 1+e^{i(k_y-k_x)} & 0 \end{bmatrix} + i\lambda_1 \begin{bmatrix} 0 & 1+e^{-ik_x} & -1-e^{-ik_y} \\ -1-e^{ik_x} & 0 & 1+e^{i(k_x-k_y)} \\ 1+e^{ik_y} & -1-e^{i(k_y-k_x)} & 0 \end{bmatrix}. \quad (7)$$

The three Bloch bands can be flattened using the projector method detailed for the Haldane model in Section II. We focus on the lowest band. Unless specified otherwise, the numerical calculations shown below are performed at $\lambda_1 = t_1$ as discussed in the original paper[32]. The lowest band has unit Chern number.

A. Filling 1/3

We fill the flattened lowest band to filling 1/3, and add density-density repulsion between NN. After the gauge transform, the interaction term reads

$$\frac{1}{N}\sum_{\{\mathbf{k}_i\}} \delta^{\mathrm{mod}2\pi}_{\mathbf{k}_1+\mathbf{k}_2-\mathbf{k}_3-\mathbf{k}_4} \sum_{\alpha<\beta}^{A,B,C} \psi^\dagger_{\mathbf{k}_3\alpha}\psi^\dagger_{\mathbf{k}_4\beta}\psi_{\mathbf{k}_2\beta}\psi_{\mathbf{k}_1\alpha} V^{\alpha\beta}_{\mathbf{k}_1\mathbf{k}_2\mathbf{k}_3\mathbf{k}_4}, \quad (8)$$

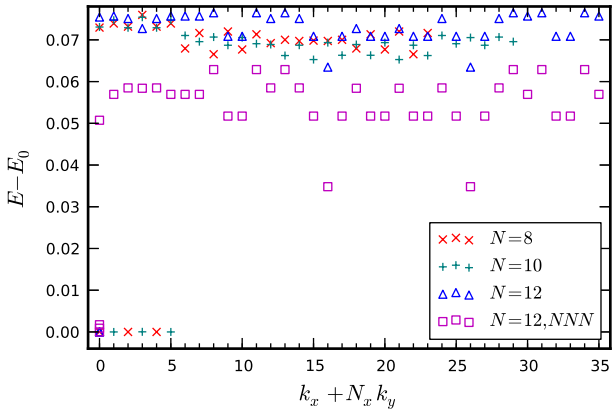

FIG. 22: Low energy spectrum of the Kagome lattice model with $N = 8$ (marked by red crosses), $N = 10$ (green plus signs), and $N = 12$ (blue triangles) particles on the $N_x \times N_y = 6 \times N/2$ lattice, with energies shifted by E_0, the lowest energy for each system size. Also shown (magenta squares) is the spectrum of $N = 12$ particles on the $N_x \times N_y = 6 \times 6$ lattice in the alternative Kagome model with NNN hoppings at the parameters suggested in the original paper[32], namely $(\lambda_1, \lambda_2, t_2) = (0.28, 0.2, -0.3)$.

where the sublattice indices (α, β) are summed over (A, B), (B, C), (C, A), and the interaction factors are

$$\begin{aligned} V^{AB}_{\mathbf{k}_1\mathbf{k}_2\mathbf{k}_3\mathbf{k}_4} &= 1 + e^{-i(\mathbf{k}_2-\mathbf{k}_4)\cdot\mathbf{b}_1}, \\ V^{BC}_{\mathbf{k}_1\mathbf{k}_2\mathbf{k}_3\mathbf{k}_4} &= 1 + e^{i(\mathbf{k}_2-\mathbf{k}_4)\cdot(\mathbf{b}_1-\mathbf{b}_2)}, \\ V^{CA}_{\mathbf{k}_1\mathbf{k}_2\mathbf{k}_3\mathbf{k}_4} &= 1 + e^{i(\mathbf{k}_2-\mathbf{k}_4)\cdot\mathbf{b}_2}. \end{aligned} \quad (9)$$

The 6 terms are illustrated by the 6 ellipses in Fig. 21.

We show the energy spectrum of $N = 8, 10, 12$ particles on the $N_x \times N_y = 6 \times \frac{N}{2}$ lattice in Fig. 22. In the three cases, a 3-fold degenerate ground state is seen at total momenta $\{(0,0),(2,0),(4,0)\}$, $\{(1,0),(3,0),(5,0)\}$, $\{(0,0),(0,0),(0,0)\}$, respectively. Again, this agrees perfectly with the $(1,3)$-admissible counting proposed in Ref. 15,22. The ratio of the gap to the energy spread of the ground-state manifold is larger than that of the Haldane model. As shown in Fig. 23, the energy gap ΔE remains open and scales to a finite value in the limit of $N \to \infty$ with N_x/N_y finite. And the three degenerate ground states exhibit spectral flow upon flux insertion. The period of 3 fluxes, shown in Fig. 24, indicates the system has Hall conductance $\sigma_{xy} = 1/3$.

We probe the quasihole excitations by the particle entanglement spectrum of the ground state. In Fig. 25, we observe a clear, *very large* entanglement gap in the spectrum, and the counting of the entanglement energy levels below the gap again matches in each momentum sector the $(1,3)$-admissible counting[15,22]. The width of the entanglement gap is $\Delta\xi = 4.64$. This means that in the ground state of the Kagome lattice model, the inter-particle correlations that obey the $(1,3)$ generalized Pauli principle is stronger than any other correlations *by two orders of magnitude!* We thus conclude that the

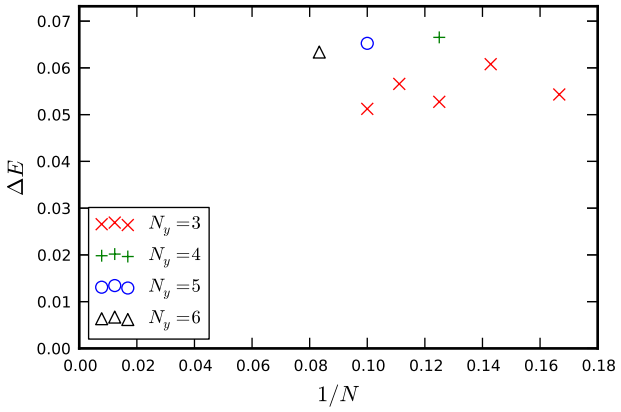

FIG. 23: Energy gap ΔE of the Kagome lattice model for different system sizes and aspect ratios. In each case, $N_x = 3N/N_y$.

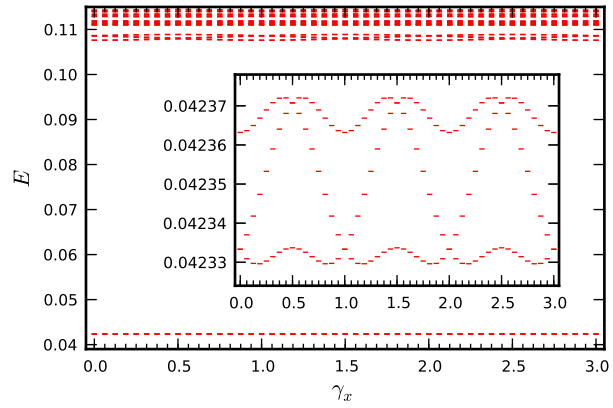

FIG. 24: Spectral flow of the low-lying states of the Kagome lattice model with $N = 10$ particles on the $N_x \times N_y = 6 \times 5$ lattice upon flux insertion along the x direction. γ_x counts the number of fluxes inserted. The 3-fold ground states flow into each other, and do not mix with higher states during flux insertion. It takes 3 full fluxes for the 3-fold states to return to the original configuration (inset).

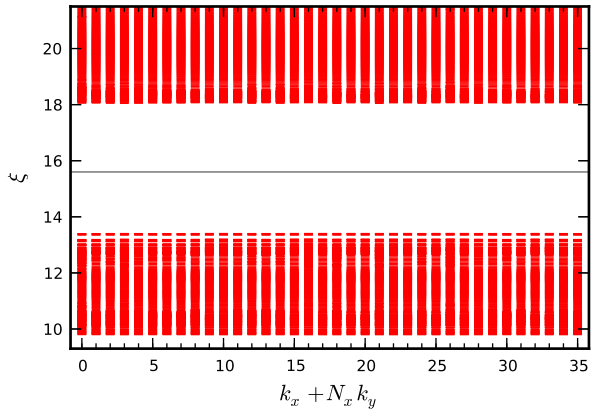

FIG. 25: Particle entanglement spectrum of the ground state of the Kagome lattice model of $N = 12$ particles on the $N_x \times N_y = 6 \times 6$ lattice, with $N_B = 7$ particles traced out. The number of states below the gray line is 2530 in each momentum sector, in agreement with the $(1, 3)$-admissible counting rule. The width of the entanglement gap is $\Delta\xi = 4.64$, meaning that spurious, non-FQH correlations have a probability of $e^{-4.64} \approx 0.0097$ relative to the universal ones.

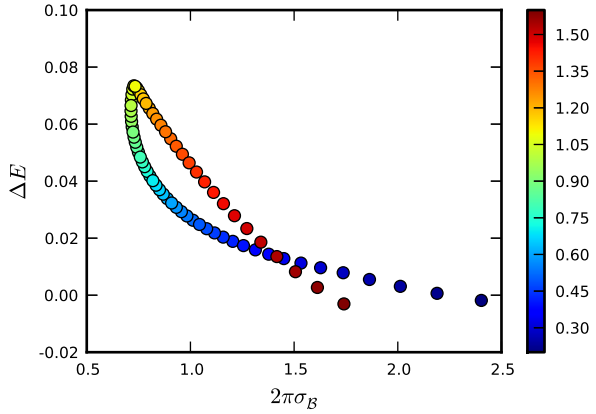

FIG. 26: The correlation between the standard deviation $\sigma_{\mathcal{B}}$ of Berry curvature and the gap ΔE in the energy spectrum of 8 particles on the $N_x \times N_y = 6 \times 4$ lattice. The calculations are performed at $t_1 = 1$. The color of each scatter point encodes the value of λ_1 per the color bar to the right. A negative correlation between $\sigma_{\mathcal{B}}$ and ΔE is visible.

ground state is a FCI state with characteristics of the FQH Laughlin state.

Now we briefly address the issue of parameter dependence. Without loss of generality, we fix $t_1 = 1$ and vary λ_1 in the range $(0, \sqrt{3})$. In this region, the single-particle spectrum is gapped and the lowest band has unit Chern number[32]. A strong correlation between the energy gap ΔE and the Berry curvature fluctuation $2\pi\sigma_{\mathcal{B}}$ on λ_1 is clearly visible in Fig. 26.

As a sanity check, we have also looked at the case where one partially fills the second band. We assume the lowest band is completely filled and inert, and diagonalize the second band directly. In such a situation, there is no evidence for Laughlin-like physics at filling $1 + 1/3$. This is expected since the second band has zero Chern number[32].

In Ref. 32, it was shown that by adding properly chosen NNN hopping terms, the band gap to bandwidth ratio can be enhanced by more than an order of magnitude, and it was argued that this alternative model could support a more robust Laughlin-like phase when interactions are added. Unfortunately, we observe the opposite effect: compared with the simple model with only NN hoppings, both the energy gap and the entanglement gap are only about half as large for the two cases with NNN hoppings studied in Ref. 32. The reduction of $\Delta\xi$ from 4.64 to 1.95 means the relative strength of the $(1, 3)$ Pauli principle exclusion is reduced by a factor of ~ 15. The energy and the entanglement spectra for the case with the largest band gap to bandwidth ratio [at $(\lambda_1, \lambda_2, t_2) = (0.28, 0.2, -0.3)$] are shown in Figs. 22

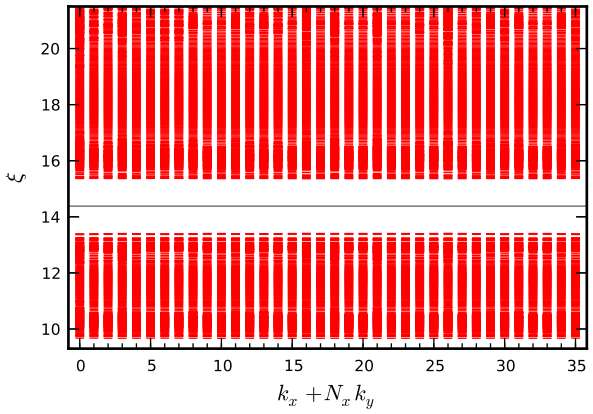

FIG. 27: Particle entanglement spectrum of the ground state of the Kagome lattice model with NNN hoppings of $N = 12$ particles on the $N_x \times N_y = 6 \times 6$ lattice at $(\lambda_1, \lambda_2, t_2) = (0.28, 0.2, -0.3)$, with $N_B = 7$ particles traced out. The number of states below the gray line is 2530 in each momentum sector, in agreement with the $(1, 3)$ counting rule. The width of the entanglement gap is $\Delta\xi = 1.95$, much smaller than the gap of the model with only NN hoppings shown in Fig. 25.

and 27. We have checked the nearby parameter region and no qualitative change is observed. Carefully tuning the NNN hoppings could achieve $\sim 10\%$ flatter Berry curvature, but the energy gap and the entanglement gap still end up smaller than the simple model with only NN hoppings, showing that the flat Berry curvature – FQH phase correspondence is to be taken as a general trend, rather than a quantitative result.

B. Half filling

Among the FQH phases, the Moore-Read (MR) state plays a special role. It is one of the best candidates to explain the experimentally observed fraction $\nu = 5/2$ and its excitations obey non-Abelian statistics. The $\mathbb{Z}_n$ Read-Rezayi (RR) states are the generalization of Laughlin ($n = 1$) and MR ($n = 2$) states. They occur at a filling factor $\nu = n/(n + 2)$. The $\mathbb{Z}_3$ RR state is a potential candidate to explain the fraction $\nu = 12/5$.

It has been recently shown that a $(n + 1)$-body short-range interaction can stabilize the analogue of a $\mathbb{Z}_n$ RR state on the checkerboard lattice[22]. The $(n + 1)$-body interaction used in Ref. 22 mimics the short range interaction for which the $\mathbb{Z}_n$ RR state is the exact zero-energy ground state with highest density. It has also been very recently demonstrated[18] that the Haldane model of hard-core bosons exhibits a MR state at filling $\nu = 1$. The three-body hard-core repulsion in that case was implemented by restricting the occupancy of any site to be less than three.

In this section, we focus on the half-filling case and thus on the fermionic MR state. Until now, we have found no evidence that a two-body NN interaction could stabilize a MR-like state in any of the lattice models studied. Instead of the two-body NN repulsion, we add to the Kagome lattice model a *three*-body NN repulsion similar to the one in Ref. 22, as shown by the gray triangles in Fig. 21. After the gauge transform, the density-density-density interaction term reads

$$\frac{1}{N}\sum_{\{\mathbf{k}_i\}} \delta^{\mathrm{mod}2\pi}_{\substack{\mathbf{k}_1+\mathbf{k}_2+\mathbf{k}_3 \\ -\mathbf{k}_4-\mathbf{k}_4-\mathbf{k}_6}} \psi^\dagger_{\mathbf{k}_4 A}\psi^\dagger_{\mathbf{k}_5 B}\psi^\dagger_{\mathbf{k}_6 C}\psi_{\mathbf{k}_3 C}\psi_{\mathbf{k}_2 B}\psi_{\mathbf{k}_1 A} \times V_{\mathbf{k}_1\mathbf{k}_2\mathbf{k}_3\mathbf{k}_4\mathbf{k}_5\mathbf{k}_6}, \quad (10)$$

where

$$V_{\mathbf{k}_1\mathbf{k}_2\mathbf{k}_3\mathbf{k}_4\mathbf{k}_5\mathbf{k}_6} = 1 + e^{-i(\mathbf{k}_2-\mathbf{k}_5)\cdot\mathbf{b}_1 - i(\mathbf{k}_3-\mathbf{k}_6)\cdot\mathbf{b}_2}. \quad (11)$$

It is well known that a short-range three-body repulsion stabilizes the Pfaffian MR FQH state[34] in a half-filled Landau level[45]. We therefore expect an analogous FCI phase appearing at half filling. The MR FQH state has fractional excitations governed by the generalized Pauli principle of having no more than 2 particles in 4 consecutive Landau level orbitals and the fermionic statistics of no more than one particle allowed per orbital[23,24]. This enables a direct extension of the $(1, 3)$-admissible FCI counting of having no more than 1 particle in 3 consecutive orbitals[15] to a $(2, 4)$-admissible counting[22] for the possible MR FCI state.

We diagonalize the interacting Hamiltonian in the flattened lowest band at filling 1/2. We show the energy spectrum of $N = 8, 10, 12$ particles on the $N_x \times N_y = \frac{N}{2} \times 4$ lattice in Fig. 28. In the three cases, a 6-fold degenerate ground state is seen at total momenta $\{6 \times (0, 0)\}$, $\{(0, 0), 2\times(0, 1), (0, 2), 2\times(0, 3)\}$, $\{2\times(0, 0), 4\times(0, 2)\}$, respectively. This agrees exactly with the $(2, 4)$-admissible counting proposed above. As shown in Fig. 29, the energy gap ΔE remains open and scales to a finite value in the limit of $N \to \infty$ with N_x/N_y finite. The six degenerate ground states exhibit spectral flow upon flux insertion. As shown in Fig. 30, the period of the spectral flow is 2 fluxes, and therefore the ground state has Hall conductance $\sigma_{xy} = 1/2$.

We probe the quasihole excitations by using the particle entanglement spectrum of the ground state. In Fig. 31, we observe a clear and large gap in the entanglement spectrum, and the counting of the entanglement energy levels below the gap again matches in each momentum sector the $(2, 4)$-admissible counting as predicted in Ref. 22. The width of the entanglement gap is $\Delta\xi = 1.66$. This indicates that the inter-electron correlations that obey the $(2, 4)$ generalized Pauli principle, i.e. the pairing of electrons, is 5 times stronger than any other kind of correlations. Therefore, we conclude that the ground state of the Kagome lattice model with the three-body NN interactions at half filling is indeed a MR FQH state.

Based on the results at filling 1/3 and 1/2, we make the conjecture that *under desirable conditions*, a short-range $(n + 1)$-body interaction could stabilize $\mathbb{Z}_n$ RR parafermion FQH state[37] in a Chern band at filling

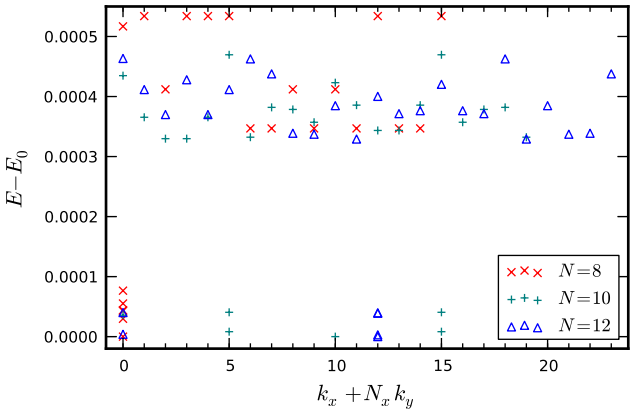

FIG. 28: Low energy spectrum of the Kagome lattice model with three-body interactions of $N = 8$ (marked by red crosses), $N = 10$ (green plus signs), and $N = 12$ (blue triangles) particles on the $N_x \times N_y = \frac{N}{2} \times 4$ lattice, with energies shifted by E_0, the lowest energy for each system size. We only show the lowest excited level in each momentum sector in addition to the 6-fold ground state.

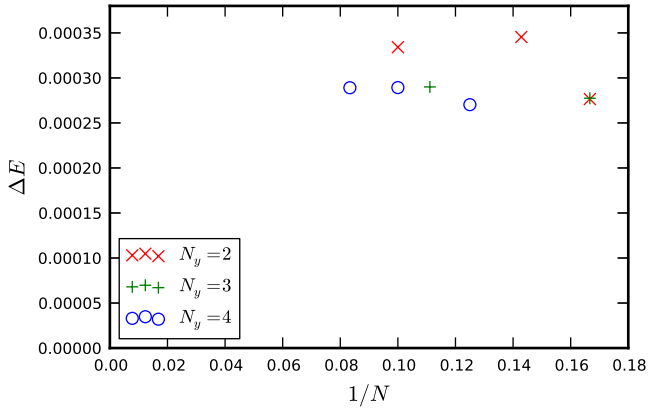

FIG. 29: Energy gap ΔE of the Kagome lattice model with three-body interactions for different system sizes and aspect ratios. In each case, $N_x = 2N/N_y$.

$n/(n+2)$. Further work is needed to confirm the cases $n \geq 3$. The $n = 3$ case has recently been reported in Ref. 22.

We have also looked for a MR phase in the Haldane and two-orbital models using three-body interactions. Unfortunately, these two models do not seem to exhibit such a phase. This appears to be consistent with the more fragile Laughlin-like phase in these models.

V. RUBY LATTICE MODEL

The last Chern insulator we have analyzed is on a ruby lattice. Hu et al.[33] have considered a two-dimensional ruby lattice with strong spin-orbit coupling. The simplified spin-polarized version of this model was shown to provide a Chern insulator with an extremely flat lowest band.

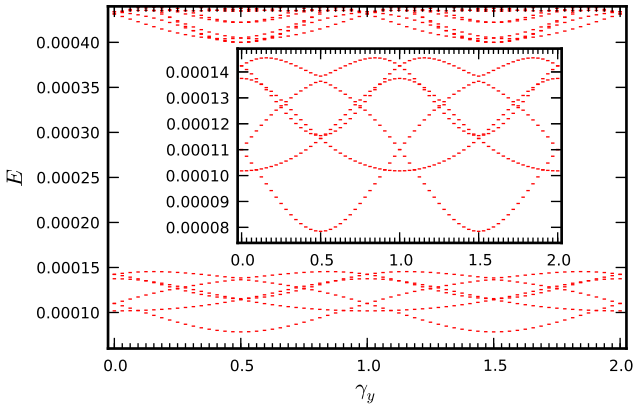

FIG. 30: Spectral flow of the low-lying states of the Kagome lattice model with three-body interaction of $N = 10$ particles on the $N_x \times N_y = 5 \times 4$ lattice upon flux insertion along the y direction. γ_y counts the number of fluxes inserted. The 6-fold ground states flow into each other, and do not mix with higher states during flux insertion. After insertion of every 2 full fluxes, the 6-fold states return to the original configuration (inset).

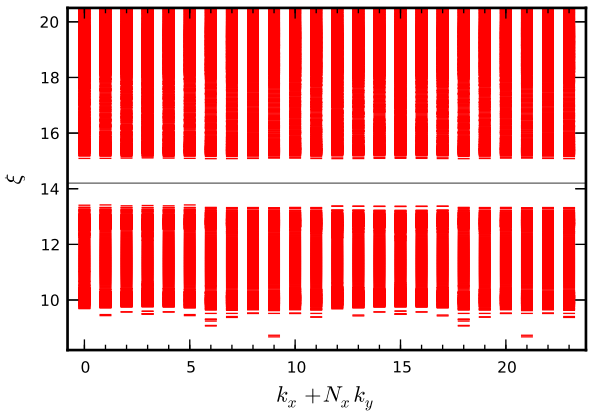

FIG. 31: Particle entanglement spectrum of the ground state of the Kagome lattice model with three-body interactions of $N = 12$ particles on the $N_x \times N_y = 6 \times 4$ lattice, with $N_B = 6$ particles traced out. The number of states below the gray line is 2910 in momentum sectors with $k_x = 1, 3$ and $k_y = 0, 2$, 2912 in sectors $(0, 0)$ and $(0, 2)$, 2940 in sectors with $k_x = 5$ and sectors with $k_x = 2, 4$ and $k_y = 2, 4$, and 2944 in all the other sectors, in agreement with the $(2, 4)$-admissible counting rule. The width of the entanglement gap is $\Delta\xi = 1.66$.

As depicted in Fig. 32, the ruby lattice is spanned by the translation vectors $\mathbf{b}_1$ and $\mathbf{b}_2$ and it is made of six sublattices, denoted from 1 to 6. After a Fourier transform and a trivial gauge transform, the single-particle Hamiltonian can be cast in Bloch form as

$$H = \sum_{\mathbf{k}} \sum_{i,j=1}^{6} \Psi^{\dagger}_{\mathbf{k},i} h_{i,j}(\mathbf{k}) \Psi_{\mathbf{k},j}. \qquad (12)$$

Here the lattice momentum $\mathbf{k} = (\mathbf{k}\cdot\mathbf{b}_1, \mathbf{k}\cdot\mathbf{b}_2) \equiv (k_x, k_y)$

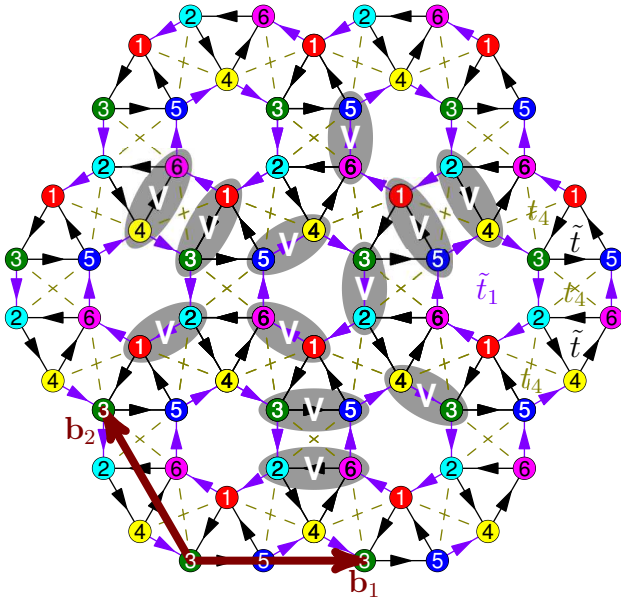

FIG. 32: The Ruby lattice model. The six sublattices 1 to 6 are colored respectively in red, cyan, green, yellow, blue and magenta. The lattice translation vectors are $\mathbf{b}_1$, $\mathbf{b}_2$. The complex hopping parameters between NN are $\tilde{t} = t_r + it_i$ for sites having the same parity (black arrows) and $\tilde{t}_1 = t_{1r} + it_{1i}$ for sites having opposite parity (purple arrows), both in the direction of the arrows. The real hopping parameter on the diagonal of the square (olive dashed lines) is given by t_4. The density-density repulsion between NN is depicted by gray ellipses.

is summed over the first Brillouin zone, and the $h(\mathbf{k})$ matrix is given by (the upper triangle can be obtained from Hermiticity)

$$h(\mathbf{k}) = -\begin{bmatrix} 0 & & & & & & \\ \tilde{t}_1^* & 0 & & & & & \\ \tilde{t} & \tilde{t}_1^* e^{-i(k_x+k_y)} & 0 & & & & \\ t_4\left(1+e^{ik_x}\right) & \tilde{t} & \tilde{t}_1^* e^{ik_x} & 0 & & & \\ \tilde{t}^* & t_4\left(1+e^{-i(k_x+k_y)}\right) & \tilde{t} & \tilde{t}_1^* & 0 & & \\ \tilde{t}_1 e^{ik_x} & \tilde{t}^* & t_4\left(e^{ik_x}+e^{i(k_x+k_y)}\right) & \tilde{t} & \tilde{t}_1^* e^{i(k_x+k_y)} & 0 & \end{bmatrix}. \quad \text{(13)}$$

We adopt the parameter values suggested in the original article[33], namely $(t_i, t_{1r}, t_{1i}, t_4) = (1.2, -1.2, 2.6, -1.2)t_r$. For these parameters, the lowest band of the problem is gapped, and has unit Chern number[33].

Again, we flatten the Bloch bands using projectors, and we add density-density repulsion of unit strength between nearest neighbors. There are 12 type of terms as depicted by the gray ellipses in Fig. 32. We diagonalize the interacting Hamiltonian in the flattened lowest band at filling 1/3 with up to $N = 12$ particles, and find results quite similar to the previous three models. Namely, we find a 3-fold degenerate ground state in the momentum sectors predicted by the $(1, 3)$ counting principle. The degenerate ground state is separated from the excitations by a finite energy gap. Finite-size scaling indicates that the gap remains open in the thermodynamic limit. Twisting boundary drives spectral flow within the ground-state manifold and the flow has a period of 3 fluxes. Hence, the system has Hall conductance $\sigma_{xy} = 1/3$. We calculate the entanglement spectra for various system sizes and find an entanglement gap with the $(1, 3)$-admissible counting in each case. As an example, we show in Fig. 33 the entanglement spectrum of the ground state of $N = 12$ particles. The entanglement gap $\Delta\xi = 5.07$ is comparable to, although slightly smaller than the entanglement gap $\Delta\xi = 5.53$ of the Kagome lattice model with only NN hoppings at the same system size. This pronounced sign of exclusion statistics counting suggests that the system has fractional excitations

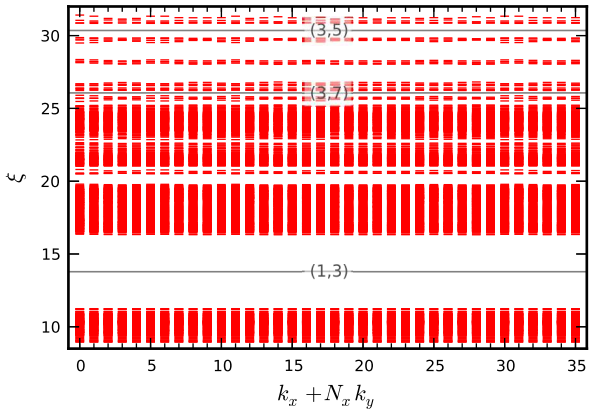

FIG. 33: Particle entanglement spectrum of the ground state of the ruby lattice model of $N = 12$ particles on the $N_x \times N_y = 6 \times 6$ lattice, with $N_B = 8$ particles traced out. The number of states below each of the three gray lines is $741, 1629, 1645$ in momentum sectors where both k_x and k_y are even and $728, 1612, 1628$ elsewhere. These numbers are in perfect accordance with the $(1,3)$-, $(3,7)$-, and $(3,5)$-admissible counting, respectively. The width of the $(1,3)$ entanglement gap is $\Delta\xi = 5.07$. The counting of levels below the unmarked gaps do not correspond to any (k,r)-admissible rule.

similar to the Laughlin quasiholes. We do however stress that we have *not* computed the statistics of the quasiholes, as this would require braiding operations likely to be plagued by finite-size effects on the lattices we can reach by computers. We conclude that the ground state of the ruby lattice model with two-body NN repulsions is a FQH Laughlin state.

We have also checked the effect of three-body NN repulsions at half filling. There are a total of 14 terms, corresponding to 2 equilateral triangles and 12 right triangles embedded in rectangles. Similar to the case of the Kagome lattice model detailed in Section IV B, we find a robust MR state here. The state has the hallmark 6-fold degenerate gapped ground state at the correct momenta. We also find a large entanglement gap corresponding to fractional excitations governed by the $(2,4)$ generalized Pauli principle.

VI. STRUCTURES IN ENTANGLEMENT SPECTRUM

As discussed in previous sections, the entanglement spectrum of the ground state of a short-range $(m+1)$-body interaction has a gap corresponding to the $(m, m+2)$-admissible counting, for $m = 1, 2$. This gap measures the prominence of m-particle clustering in the ground state. The $(m+1)$-body interactions could possibly generate clusters of other sizes as well. For example, in the FQH effect in the continuum, MR states can be obtained with just two-body potentials. In that case, there could be additional gaps in the entanglement spectrum, and the counting of levels below these gaps could conform to other generalized Pauli principles.

The appearance of a $(n, n+r)$-admissible counting reveals the existence of a specific clustering pattern in the ground state. This pattern is also present in the model fermionic FQH state at filling $\nu = n/(n+r)$ described by the (n,r) Jack polynomials multiplied by a Vandermonde determinant[23,24]. For example, a $(n, n+2)$-admissible counting corresponds to the $\mathbb{Z}_n$ Read-Rezayi FQH state[37], and a $(2,5)$-admissible counting corresponds to the 'Gaffnian' FQH wave function[46]. The model wave functions of such FQH states have characteristic zeros when a cluster of $n+1$ particles forms even after removing the "trivial" zeros provided by the fermionic statistics. This reflects specific $(n+1)$-body correlations in the system. Therefore, the presence of a gap with a $(n, n+r)$ admissible counting in the FCI entanglement spectrum signals the presence of clustering correlations similar to a specific model FQH state, and implies the presence of stable $(n+1)$-body correlations in the system.

We check comprehensively all the four models studied in this paper as well as the checkerboard lattice model[15,47], at various system sizes up to $N = 12$ particles. In most cases, we find extra entanglement gaps other than the one above the states of $(m, m+2)$-admissible counting in the ground state of an $(m+1)$-body interaction, and the counting of entanglement energy levels below *some* of these gaps matches with an $(n, n+r)$-admissible counting in each momentum sector. For all the systems we look at, we usually find at least one such extra gap that matches perfectly with a particular $(n, n+r)$-admissible rule. For example, in the Kagome lattice model with two-body interaction, we find two extra entanglement gaps in the ground state (Fig. 34), with the counting of levels below them given *exactly* (in each momentum sector) by the $(2,4)$- and $(2,5)$-admissible counting and the folding based on the FQH-FCI mapping[22]. The former case corresponds to the MR state while the latter corresponds to the Gaffnian wave function. We find the appearance of the counting of non-Abelian statistics in the Laughlin-like ground state of two-body interactions quite intriguing.

We do not have a complete understanding of the full gap structure at the moment. In the earlier example of the ruby lattice model shown in Fig. 33, we find a few extra entanglement gaps. Two of them have counting below the gap given *exactly* (in each momentum sector) by $(3,5)$- and $(3,7)$-admissible rules[22] respectively, the former of which corresponds to a $\mathbb{Z}_3$ Read-Rezayi state. There are other entanglement gaps in the spectrum that cannot be explained by any $(n, n+r)$-admissible rule.

All of such extra $(n, n+r)$ entanglement gaps that we observe have $n+1 = N_A$, where N_A is the number of particles left in the system when evaluating the entanglement spectrum. Tracing out part of the system enhances the correlation between the remaining N_A particles. One can imagine that such enhancement is more significant for the correlation between the N_A particles as a whole

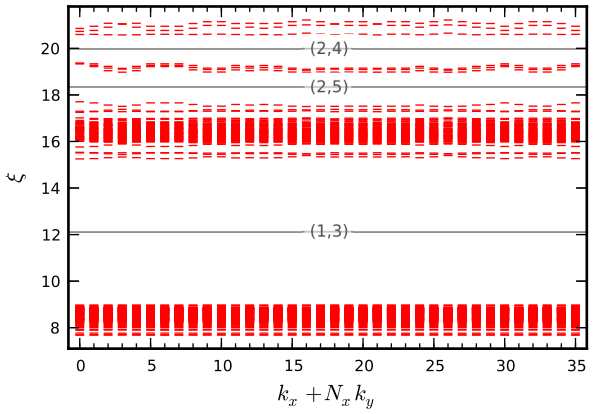

FIG. 34: Particle entanglement spectrum of the ground state of the Kagome lattice model of $N = 12$ particles on the $N_x \times N_y = 6 \times 6$ lattice, with $N_B = 9$ particles traced out. The number of states below each of the three gray lines is $138, 195, 198$ in momentum sectors where $k_x, k_y \in \{0, 3\}$ and $135, 192, 195$ elsewhere. These numbers are in perfect accordance with the $(1, 3)$-, $(2, 5)$-, and $(2, 4)$-admissible counting, respectively.

than the correlation within a fraction of the N_A particles. In most cases, we observe such (N_A-1, N_A-1+r) entanglement gaps for almost every value of N_A. Our examples show that a ground-state wave function at $\nu = 1/3$ can give us information about possible non-Abelian correlations.

This suggests a feature of the FCI: the $(n + 1)$-body interacting Hamiltonian could not only generate strong $(n + 1)$-body correlations, but also higher-body correlations. This gives hope for the possible realization of other members of the Read-Rezayi series with two-body potentials. It is very intriguing that entanglement in the ground state of an $(n+1)$-body interacting Hamiltonian at filling $\nu = n/(n + 2)$ contains clear clues that some other FQH states could possibly be stabilized by some *other* interaction at some *other* filling.

VII. DISCUSSION AND CONCLUSION

In this paper, we have studied four examples of flat-band Chern insulators. If we include the previous articles[13–15,17] on the checkerboard lattice, we now have five cases which can be used to compare the universal physics.

First, we have showed that the existence of FCI does not require a special lattice. Under proper conditions, FCI phases could (at least) emerge from lattice models with 2, 3, or 6 sites per unit cell. There is no restriction on the type of Bravais lattice either.

Second, we find concrete evidence that the stability of the FCI phase is not guaranteed by flat band dispersion. A large enough gap to bandwidth ratio is necessary for the existence of an insulating state at a fractional filling. Our calculations performed in the flat-band limit do not capture this effect. However, our results reveal that the single-particle eigenstates play a critical role in the formation of a FCI state as well; a badly chosen parameter set could destroy the topological phase even when the band dispersion is perfectly flat. The example of the Kagome model is especially instructive. While the addition of NNN hopping terms could make the band flatter, it actually deteriorates the FCI phase. Thus the search of a realistic FCI that would include the effect of the band dispersion relation, should not focus only on the flat-band criterion.

Third, the development of a FCI state is often dependent on suppressed fluctuations in the Berry curvature. This agrees qualitatively with the picture derived from the algebra of projected density operators. It should be noted, however, that even the suppressed curvature fluctuations could actually be considerably strong.

Fourth, out of the five models that we have checked, the Kagome lattice model with only NN hoppings has the most robust FCI phase. The ruby lattice model comes close, but has three more tunable parameters.

In conclusion, we have established the existence of a FCI phase in four distinct flat-band lattice models at filling $\nu = 1/3$ with short-range repulsive density-density interactions. The FCI phase is identified by an incompressible ground state with Hall conductance $\sigma_{xy} = 1/3$ and excitations obeying the same counting as Laughlin quasiholes. We have observed that in some cases, band structures that favor the emergence of the FCI phase have less fluctuating Berry curvature. In the presence of short-range three-body repulsive interactions, we have also found another FCI phase reminiscent of the Pfaffian Moore-Read FQH state at half filling of the Kagome lattice model and the ruby lattice model, in addition to the previously known example of the Moore-Read phase in the checkerboard lattice model. This more exotic phase has an incompressible ground state with Hall conductance $\sigma_{xy} = 1/2$ and excitations exhibiting the counting of Moore-Read quasiholes. On the technical side, we have demonstrated from various angles the power of the entanglement spectrum as a sensitive and reliable probe of topological order, when no model wave functions are available. We have also discussed interesting structures in the entanglement spectrum and their implication for the possible stable existence of other FQH states at zero magnetic field. Future directions for this line of research include strongly interacting Chern insulators with Chern number higher than one, such as the dice model[48].

VIII. ACKNOWLEDGEMENTS

BAB wishes to thank Z. Papic, F.D.M. Haldane, T.L. Hughes, S.L. Sondhi, and S.A. Parameswaran for useful discussions. NR acknowledges fruitful discussions with G. Moeller. BAB was supported by Princeton Startup Funds, NSF CAREER DMR-095242, ONR - N00014-11-1-0635, DARPA - N66001-11-1-4110 and NSF-MRSEC DMR-0819860 at Princeton University.

YLW was supported by NSF CAREER DMR-095242. BAB thanks Technion, Israel, and Ecole Normale Superieure, Paris, for generous hosting during the stages of this work.

[1] F. D. M. Haldane, Physical Review Letters **61**, 2015 (1988).
[2] C. L. Kane and E. J. Mele, Physical Review Letters **95**, 146802 (2005).
[3] C. L. Kane and E. J. Mele, Physical Review Letters **95**, 226801 (2005).
[4] B. A. Bernevig and S.-C. Zhang, Physical Review Letters **96**, 106802 (2006).
[5] B. A. Bernevig, T. L. Hughes, and S.-C. Zhang, Science **314**, 1757 (2006).
[6] M. König, S. Wiedmann, C. Brüne, A. Roth, H. Buhmann, L. W. Molenkamp, X.-L. Qi, and S.-C. Zhang, Science **318**, 766 (2007).
[7] D. Hsieh, D. Qian, L. Wray, Y. Xia, Y. S. Hor, R. J. Cava, and M. Z. Hasan, Nature **452**, 970 (2008).
[8] M. Hasan and C. Kane, Reviews of Modern Physics **82**, 3045 (2010).
[9] M. Z. Hasan and J. E. Moore, Annual Review of Condensed Matter Physics **2**, 55 (2011).
[10] A. P. Schnyder, S. Ryu, A. Furusaki, and A. W. W. Ludwig, Physical Review B **78**, 195125 (2008).
[11] X.-L. Qi, T. L. Hughes, and S.-C. Zhang, Physical Review B **78**, 195424 (2008).
[12] A. Kitaev, AIP Conference Proceedings **1134**, 22 (2009).
[13] T. Neupert, L. Santos, C. Chamon, and C. Mudry, Physical Review Letters **106**, 236804 (2011).
[14] D. N. Sheng, Z.-C. Gu, K. Sun, and L. Sheng, Nature Communications **2**, 389 (2011).
[15] N. Regnault and B. A. Bernevig, ArXiv e-prints (2011), 1105.4867.
[16] J. W. F. Venderbos, S. Kourtis, J. van den Brink, and M. Daghofer, ArXiv e-prints (2011), 1109.5955.
[17] Y.-F. Wang, Z.-C. Gu, C.-D. Gong, and D. N. Sheng, Physical Review Letters **107**, 146803 (2011).
[18] Y.-F. Wang, H. Yao, Z.-C. Gu, C.-D. Gong, and D. N. Sheng, ArXiv e-prints (2011), 1110.4980.
[19] T. Neupert, L. Santos, S. Ryu, C. Chamon, and C. Mudry, Physical Review B **84**, 165107 (2011).
[20] L. Santos, T. Neupert, S. Ryu, C. Chamon, and C. Mudry, ArXiv e-prints (2011), 1108.2440.
[21] T. Neupert, L. Santos, S. Ryu, C. Chamon, and C. Mudry, ArXiv e-prints (2011), 1110.1296.
[22] B. A. Bernevig and N. Regnault, ArXiv e-prints (2011), 1110.4488.
[23] B. A. Bernevig and F. D. M. Haldane, Physical Review Letters **100**, 246802 (2008).
[24] B. A. Bernevig and F. D. M. Haldane, Physical Review Letters **101**, 246806 (2008).
[25] S. A. Parameswaran, R. Roy, and S. L. Sondhi, ArXiv e-prints (2011), 1106.4025.
[26] G. Murthy and R. Shankar, ArXiv e-prints (2011), 1108.5501.
[27] S. M. Girvin, A. H. MacDonald, and P. M. Platzman, Physical Review B **33**, 2481 (1986).
[28] X.-L. Qi, Physical Review Letters **107**, 126803 (2011).
[29] Y. M. Lu and Y. Ran, ArXiv e-prints (2011), 1109.0226.
[30] J. McGreevy, B. Swingle, and K. A. Tran, ArXiv e-prints (2011), 1109.1569.
[31] A. Vaezi, ArXiv e-prints (2011), 1105.0406.
[32] E. Tang, J.-W. Mei, and X.-G. Wen, Physical Review Letters **106**, 236802 (2011).
[33] X. Hu, M. Kargarian, and G. A. Fiete, Physical Review B **84**, 155116 (2011).
[34] G. Moore and N. Read, Nuclear Physics B **360**, 362 (1991).
[35] H. Li and F. D. M. Haldane, Physical Review Letters **101**, 010504 (2008).
[36] A. Sterdyniak, N. Regnault, and B. A. Bernevig, Physical Review Letters **106**, 100405 (2011).
[37] N. Read and E. Rezayi, Physical Review B **59**, 8084 (1999).
[38] R. B. Laughlin, Physical Review Letters **50**, 1395 (1983).
[39] A. Chandran, M. Hermanns, N. Regnault, and B. A. Bernevig, ArXiv e-prints (2011), 1102.2218.
[40] O. S. Zozulya, M. Haque, K. Schoutens, and E. H. Rezayi, Physical Review B **76**, 125310 (2007).
[41] M. Haque, O. Zozulya, and K. Schoutens, Physical Review Letters **98**, 060401 (2007).
[42] M. Haque, O. S. Zozulya, and K. Schoutens, Journal of Physics A: Mathematical and Theoretical **42**, 504012 (2009).
[43] M. O. Goerbig, ArXiv e-prints (2011), 1107.1986.
[44] D. Podolsky and J. Avron, private communication.
[45] M. Greiter, X.-G. Wen, and F. Wilczek, Physical Review Letters **66**, 3205 (1991).
[46] S. H. Simon, E. H. Rezayi, N. R. Cooper, and I. Berdnikov, Physical Review B **75**, 075317 (2007).
[47] K. Sun, Z. Gu, H. Katsura, and S. Das Sarma, Physical Review Letters **106**, 236803 (2011).
[48] F. Wang and Y. Ran, ArXiv e-prints (2011), 1109.3435.